Enhanced thermal performance of phase change material stabilized with textile-structured carbon scaffolds

Nan Sheng,[a] Zhonghao Rao,[a] Chunyu Zhu, [a,b] * Hiroki Habazaki [b]

[a] Jiangsu Province Engineering Laboratory of High Efficient Energy Storage Technology and Equipments & School of Electrical and Power Engineering; China University of Mining and Technology, Xuzhou, 221116, China

[b] Faculty of Engineering, Hokkaido University, Sapporo 060-8628, Japan

Corresponding Author: Chunyu ZHU
E-mail: zcyls@cumt.edu.cn and chunyu6zhu@eng.hokudai.ac.jp

Abstract:

The development of thermal conductive and porous supporting scaffolds is believed to solve the problems of poor shape-stability and low thermal conductivity of solid-liquid transition-type phase change materials (PCMs), which are promisingly used for solar thermal energy storage and management. In this paper, textile-structured carbon scaffolds with flexible shape and high porosity are produced by the direct carbonization of cotton cloth. The carbon textile with versatilely changeable shape can be employed as good conductive and supporting scaffolds for PCMs, and paraffin PCM is evaluated. The composite PCMs exhibit good shape-stability and enhanced thermal transfer properties. The composites can present anisotropically improved thermal conductivity by aligning the carbon sheets in their main yarn direction. The thermal conductivity of the composite with a carbon weight ratio of 16.5wt% is increased to 0.99 W K^{-1} m^{-1} from the main yarn direction and 0.68 W K^{-1} m^{-1} from the through sheet direction, which is greatly higher than the value of paraffin (0.25 W k^{-1} m^{-1}), and the composite show heat capacity of 170 J g^{-1}. With the facile production of flexible and shapeable carbon supporting scaffold, the high thermal storage capability, good shape-stability and high heat transfer property, the composite PCM has great potential applications in solar thermal energy storage.

Keywords: phase change material; solar thermal energy storage; carbon; heat transfer; thermal management

1. Introduction

Accompanying with the growing serious environmental problems and energy crisis, the efficient use of renewable energies, such as solar energy and wind energy, and the industrial waste heat recovery have gained increasing attentions. However, solar energy and the industrial waste heat are discontinuous and vary with period of generation. Several energy storage techniques, such as batteries and thermal energy storage (TES), have been proposed to alleviate the mismatch between peaks of energy supply and demand. TES with the use of latent heat phase change material (PCM) is especially promising, in which thermal energy is reserved or released during the melting or solidifying phase transition process of a PCM. [1-3] So far, the organic solid-liquid PCMs, such as fatty acids [4], polyethylene glycol [5, 6], erythritol[7], and paraffin wax (PW) [8], have been widely studied because of their high energy storage density, constant phase transition, good thermal stability and low supercooling degree. In spite of the great potential in improving the efficiency of thermal energy use, practical applications of organic PCMs have been hindered by their low thermal conductivity and the leakage problem in the molten state.

To enhance the thermal conductivity of organic PCMs, high thermal conductive powdery fillers, such as metals, expanded graphite, carbon nanotube, carbon fibers, graphene and ceramic powders are added to form phase change composites (PCCs). [9-14] However, the resulting PCCs only show moderate thermal conductivities because of the difficulty in forming three-dimensional (3D) continuous thermal conductive network, especially when low contents of fillers are added. Moreover, the distribution of the dispersed fillers is unstable in the PCCs when solid-liquid phase transition occurs. For simultaneously increasing the thermal conductivity and avoiding the leakage of liquified PCMs, the use of preconstructed porous supporting frameworks, which are consisted of highly thermal conductive materials, is a good strategy to fabricate form-stable PCCs with enhanced thermal conductivity. Until now, metal foams, graphene aerogels, BN foams, carbon foams, and carbon nanotube (CNT) sponges have been used employed for enhancing the performance of PCCs.[15-21] Although metal foams can greatly enhance the thermal conductivity, the use of metal foams inevitably increase the weight of PCCs, leading to low thermal storage density per unit mass. The low-weight carbon-based porous frameworks such as CNT sponges and graphene aerogels are promising supporting scaffolds to form high-performance PCCs; [15, 17, 19] however, the inherent shortcomings, including tedious preparation, low yield, high-cost and difficulty in controlling the structure, have obstructed their wide applications in thermal energy storage. Therefore, it still remains a challenge to directly prepare porous 3D carbon supporting scaffold by a facile and low-cost

strategy.

Cotton is a kind of soft and fluffy natural fiber that comes from the seedpod of the cotton plant. Cotton has been used to make a lot of textile products that are soft and breathable. The use of cotton for fabric is known to date to prehistoric times. Thanks to development of cotton textile, human's life and civilization has been greatly improved. The cotton fiber is almost pure cellulose, which is a kind of polysaccharide with a formula of $(C_6H_{10}O_5)_n$. The cotton fiber is hollow in the center. The pyrolysis of cotton fiber balls induced the formation of carbon fiber aerogels, which are consisted of hollow carbon fibers. These carbon fiber aerogels are useful absorbent for organic pollutants, which utilize the multiscale porous features. [22, 23] The hollow tubular structure of a single pyrolyzed cotton fiber inspires us that it can be a good supporting material for stabilizing organic PCM. Additionally, a textiled carbonized cotton fabric can further offer a multiscale and hierarchical porous structure for absorbing PCM, including the hollow tubular space, the spaces between the fibers and the spaces between the yarns. Therefore, in this study, we employ the carbonized cotton fabric as the supporting and thermal conductive scaffold for organic PCM. The carbonized cotton fabric has the characteristics of multiscale porous structure, good flexibility and diverse shapeability, illustrating that the cotton textile-derived carbon fabric is an ideal scaffold for fabricating PCCs with expected shape-stability and enhanced thermal conductivity. The new PCCs may have a wide application for thermal energy storage and management, especially for solar thermal energy storage.

2. Experimental

2.1 Raw materials and chemicals

A 100% cotton T-shirt with a typical rib stitch was purchased from GUNZE LIMITED (YV0215N). PW was provided by Kishida Chemical Co., Ltd.

2.2 Preparation of carbon textile and PCCs

Firstly, a piece of a 100% cotton T-shirt was used as the raw material. The cotton cloth was pyrolyzed and carbonized under Ar flow at 2400 ºC. In this manner, the flexible carbon textile (carbon cloth) was directly obtained, as shown in Figure 1a.

The carbon cloth was rolled to a cylinder, which was used for the vacuum impregnation of

PW by heating at 100 ºC. After cooling to room temperature, the PCC was prepared.

In order to evaluate the effect of density of carbon scaffold on the thermal conductivity of the PCC, a series of carbon scaffolds with different densities were prepared, as shown in Figure 1b. Different sheets (30 or 42) of carbon cloth were pressed in a module to make the same thickness of 13 mm. Subsequently, the pressed carbon scaffolds were vacuum impregnated with PW. Two PCCs were fabricated, which were named as C30@PW and C42@PW, respectively. The PCCs were cut and shaped to 10 mm disks for thermal conductivity measurement. The measurement was conducted from the main yarn direction and the through sheets direction, as shown in Figure 1b.

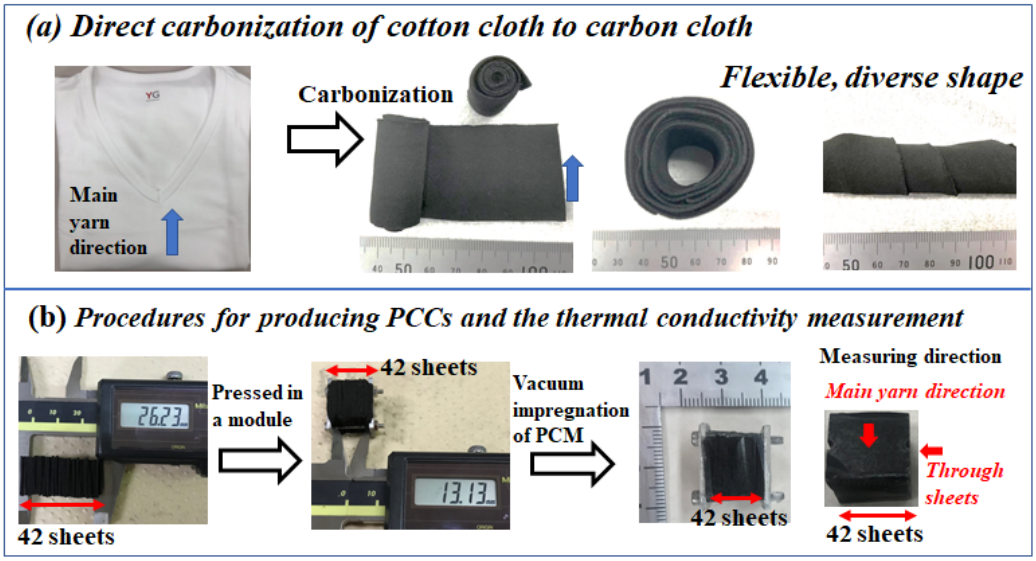

Figure 1. Schematic diagram for (a) the preparation of carbon cloth by the direct carbonization of cotton cloth and (b) the preparation of PCCs for thermal conductivity measurement.

2.3 Characterization

The X-ray diffraction (XRD) patterns of the samples was performed on an X-ray diffractometer (Rigaku Miniflex with a Cu-Kα radiation). The micro morphology of cotton textile, carbon textile and PCCs was observed by a scanning electron microscope (SEM, ZEISS, Sigma-500). The microstructure of the carbonized cotton textile was also analyzed by transmission electron microscopy (TEM, JEM-2010F). The thermal gravimetric (TG, NETZSCH STA 2500 Regulus) analysis under air flow was carried out on the PCCs and carbon cloth. The thermal conductivity of the samples was measured using a thermal conductivity

analyzer. The Fourier transform infrared (FT/IR) spectra of the samples were obtained using a FT/IR 660Plus spectrometer. The rate of thermal response of the PCCs was recorded by an infrared camera. The phase change temperature and latent heat of the samples was obtained by a differential scanning calorimeter (DSC) at a heating/cooling rate of 10 °C min^{-1} from 0 to 100 °C. The form stabilized performance of the PCCs in comparison with PW was examined by heating the samples to 80 °C for a certain duration.

3. Results and discussion

3.1 Preparation and characterization of carbon textile and PCCs

A 100% cotton T-shirt was pyrolyzed and carbonized under Ar atmosphere to obtain the carbon textile directly. Figure 2a presents the photograph of the cotton T-shirt. The cotton T-shirt has a typical rib stitch textile structure, and the yarns have a higher density in the vertical direction, denoted as main yarn direction in this study. Figure 2b shows the SEM image of the pristine cotton cloth. The cotton fibers are twisted to form yarns, and the yarns are weaved to form the cotton textile. A close observation of a single cotton fiber in Figure 2c indicates that the fiber is hollow in the center. After carbonization, the cotton textile turns black, as shown in Figure 1a. Additionally, the carbonized cotton T-shirt also presents good flexibility. It can be twisted or rolled to form a diverse structure, making it a good scaffold for absorbing organic PCMs. Figures 2d and e show the SEM images of the carbonized cloth. A well textiled carbon cloth similar to the original cotton cloth is obtained, in which the hollow carbon fibers are twisted to form yarns and the yarns are weaved to form the carbon cloth. In this way, the carbon textile contains a multiscale and hierarchical porous structure including the hollow tubular holes, the spaces between the carbon fibers and the spaces between the yarns. The hierarchical porous structure is useful for absorbing and storing organic PCM. The carbon fibers are well crystallized at a carbonization temperature of 2400 °C as-evidenced by the high resolution TEM in Figure 2f, which presents many fringes of graphite (002) planes. The XRD pattern of the carbonized sample is shown in Figure 3, presenting two distinct peaks corresponding to carbon (002) and (100) planes, respectively.

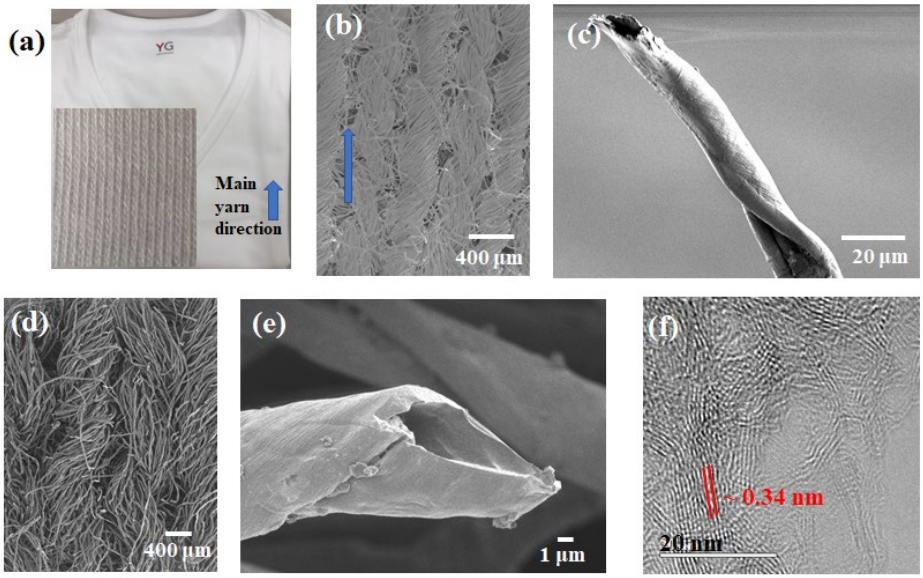

Figure 2. Morphology and microstructure observation. (a) the optical picture of the original cotton cloth from a T-shirt; (b, c) SEM images of the original cotton cloth; (d, e) SEM images of the carbonized cloth 2400 °C; (f) the high-resolution TEM image of the carbonized sample at 2400 °C.

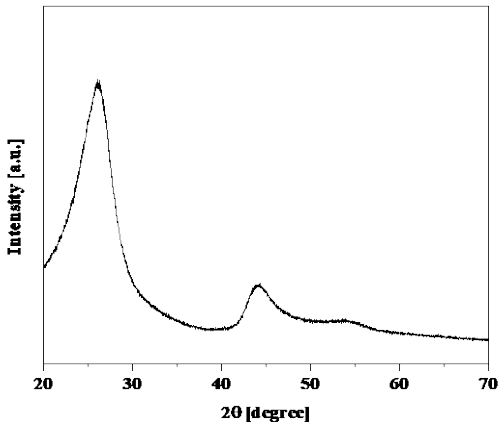

Figure 3. XRD pattern of the carbonized cotton cloth at 2400 °C.

PCCs were prepared by vacuum impregnation method. The melted PW was very easily to be infiltrated into the spaces and pores of the carbon cloth scaffolds with the assistance of heating under vacuum condition. Figure 4 presents the SEM images of the PCCs. It is observed that PW is filled in the porous spaces and holes of the carbon cloth and hollow fibers.

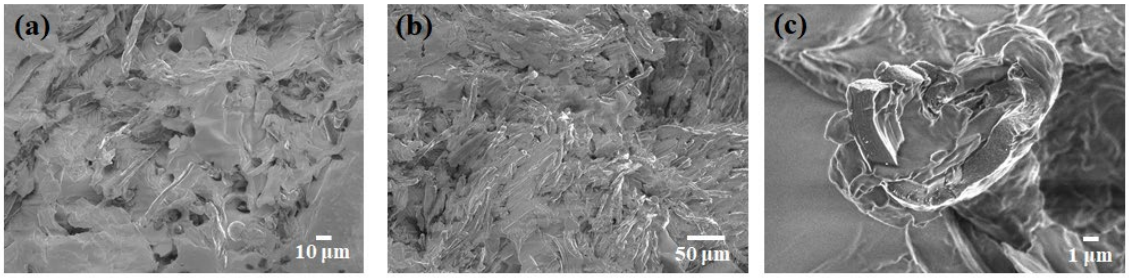

Figure 4. SEM images of the paraffin/carbon composites.

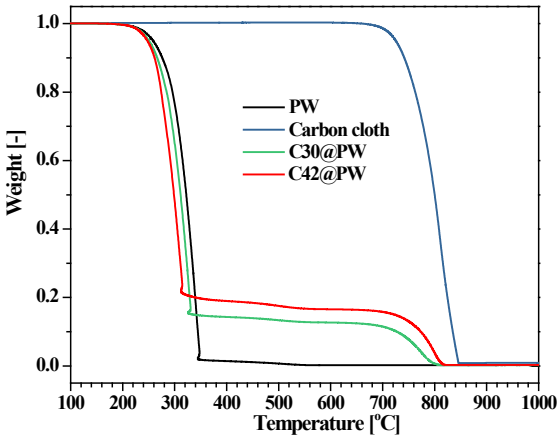

Figure 5. TG curves for the PCC samples obtained under air flow in comparison with the carbon cloth and PW.

TG measurement under air flow was carried out to determine the PW impregnation weight ratio in the PCCs. Figure 5 shows the TG curves of the PCCs, PW and carbon cloth. The carbon cloth is combusted from around 670 to 850 °C, while the combustion of PW is started from around 200 °C and finished at 350 °C. As for the PCCs, two weight decreases in the temperature ranges of 200~350 and 670~850 °C are observed, which correspond to the combustion of PW and carbon support, respectively. Based on these weight changes, the PW contents are determined to be 87.4% and 83.5% for C30@PW and C42@PW, respectively. These weight ratios are similar to those as-calculated from the weight change of carbon cloth scaffold before and after impregnating PCM.

3.2 Thermal conductivity and heat transfer properties of PCCs

The thermal conductivity of organic PCMs is very low and the value for PW is 0.25 W k^{-1} m^{-1}. The low thermal conductivity of organic PCMs could reduce the rate of heat absorption and release, therefore, their practical application of organic PCMs is quite restrained. Carbon

materials are good thermal conductive fillers for increasing the thermal conductivity. Additionally, a well-structured 3D network of the thermal conductive filler is surely effective to enhance the thermal conductivity. The thermal conductivity was measured, and the results are summarized in Figure 6a. With the introduction of the carbon supporting scaffolds, the thermal conductivity is greatly increased as compared with PW. The thermal conductivity from the through sheet direction are 0.41 and 0.68 W K^{-1} m^{-1} for samples C30@PW and C42@PW, while the values from the main yarn direction are 0.63 and 0.99 W K^{-1} m^{-1}, respectively. With the increase of the density of carbon framework, the thermal conductivity is much more increased, indicating that the carbon network is acting as the thermal conducting pathway. In addition, the PCCs also present anisotropic thermal conductivity. The thermal conductivity in the main yarn direction is much higher than (about 1.5 times) in the through sheet direction. This is because of that from the main yarn direction the yarns consisting of twisted carbon fibers offer continuous thermal conducting path along the carbon yarns, however in the through sheet direction, the thermal conduction is somewhat disturbed by the interface gaps between the carbon sheets.

In order to directly observe the thermal absorption and dissipation rates of the PCCs from both the main yarn direction and the through sheet direction, the transient temperature responses of the PCCs during heating and cooling processes were recorded by using an infrared camera. Figures 6b and c present the temperature distribution images during heating and cooling, respectively. For the heating process, two PCC blocks were put on a pre-heated ceramic plate at 80 °C and the temperature images were taken at different heating durations. For the cooling process, two blocks were firstly heated at 80 °C for the same duration, which were then quickly transferred to a cool ceramic plate at room temperature for obtaining the thermal response images during cooling. Obviously from these images, the PCC block observed from the main yarn direction shows faster thermal responses than that observed from the through sheet direction. This further confirms the conclusion that the PCC has a higher thermal conductivity from the main yarn direction than from the through sheet direction.

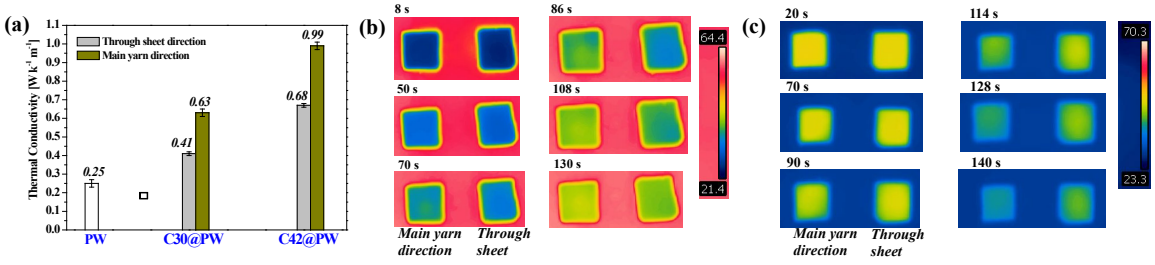

Figure 6. The thermal conduction properties. (a) Thermal conductivity of the PCCs in comparison with PW. (b, c) Thermal images of the C42@PW during heating and cooling,

respectively, in which the thermal images observed from the main yarn direction and the through sheet direction are compared.

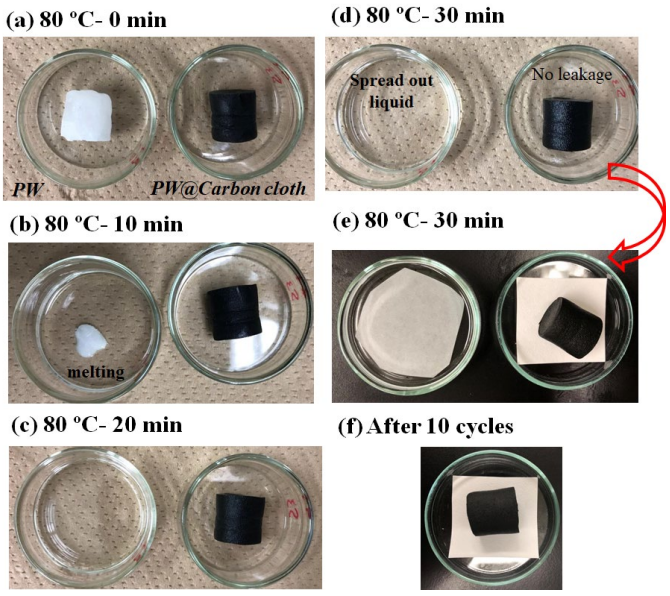

Figure 7. Leakage test of the PCC and PW. The photographs for the samples heated at 80 °C to different durations are shown in (a-e); the picture for the PCC solidified and melted for 10 cycles (f).

3.3 Leakage-proof properties of the PCCs.

Leakage-proof is an important property of PCCs for TES. The leakage test was conducted by comparing the PCC and PW which were heated at above the melting point of paraffin. Figure 7 shows the photographs of the samples heated at 80 °C for different durations. Two solid blocks are observed in their initial stages in Figure 7a. After several minutes of heating, PW begin to melt and strain the container, as shown in Figure 7b. After 20 minutes of heating as shown in Figure 7c, the liquified paraffin for PW sample spread out the container and no solid paraffin can be observed. However, there is no change for composite PW@Carbon cloth during the heating. Even after 30 minutes of heating, although paraffin should be completely melted, there is no leakage of liquid paraffin from the black composite block, as shown in Figure 7d and e. The composite PCM can also keep its original shape without obvious leakage after repeated solidification and melting, as shown in Figure 7f. In conclusion, the liquified paraffin can be well confined in the porous supporting framework. This must be caused by the capillary and surface tension forces of the porous framework to the liquid paraffin. [17, 19]

3.4 Thermal physical properties of the PCCs and PW

The thermal properties including phase transition temperatures and latent heat capacities of the samples were measured by DSC analysis. The measurement was carried out at 5 ^{o}C min^{-1} for both the heating and cooling processes. Every sample was cycled to 100 cycles. Figures 8a and c show the DSC curves for the PCCs and PW at different cycles. The DSC curves in the 100 cycles can almost overlap for PW and PCCs. This indicates the good cycling stability of the phase changes of the PW and PCCs. There are two peaks of phase changes during both the melting and solidification processes for all samples. These two peaks represent the typical solid-solid and solid-liquid phase transitions of paraffin. It is also observed that the melting curves of the PCCs shift to higher temperature side and the solidification curves shift to lower temperature side, as compared with PW. This is caused by the confinement effect of the porous supporting framework.[16, 24] The comparison of the detailed phase change temperatures, including the onset/peak melting and solidification temperatures, and phase change enthalpies of the samples are summarized in Table 1. PW has melting/solidification enthalpies of 217.7/215.4 J g^{-1}, while these values are decreased to be 182.8/179.6 J g^{-1} and 173.9/170.5 J g^{-1} for samples C30@PW and C42@PW, respectively. The reduced enthalpies for the PCCs compared with PW are caused by the addition of carbon supporting scaffolds. The samples also show good stability of enthalpies upon melting-solidification cycling. Figure 8d presents the typical enthalpies changes upon cycling. During the 100 cycles of melting and solidification, the enthalpies are almost kept constant. Besides the above good phase change stability of the paraffin PCMs, these samples also present good structure stability upon cycling.

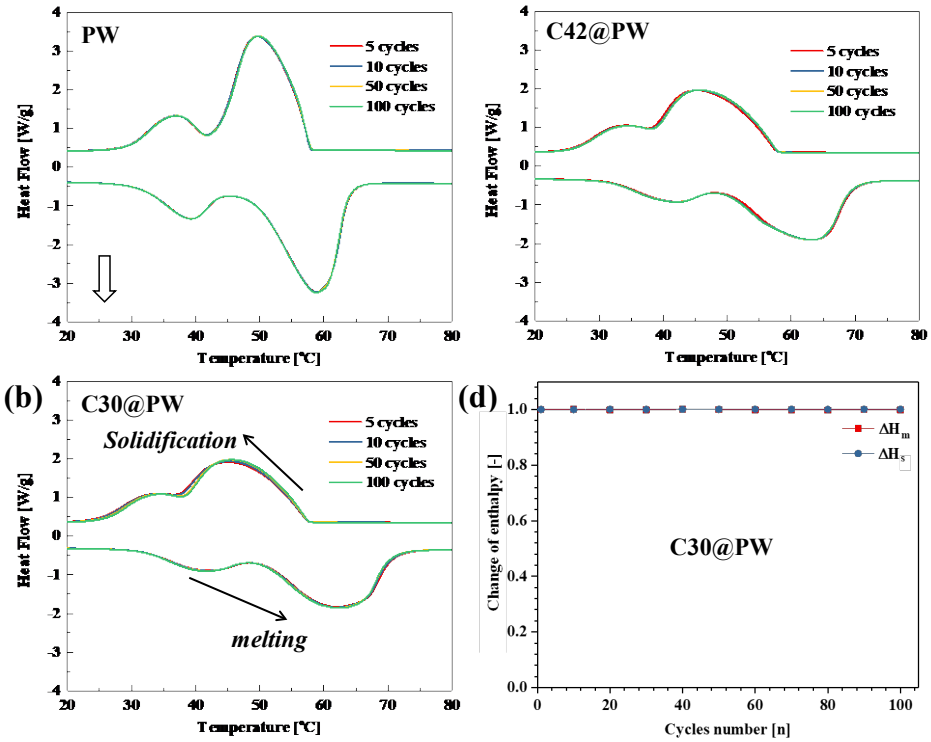

Figure 8. Thermal physical properties of the PCCs and PW. (a, b, c) DSC curves of the melting and cooling processes; (d) the typical enthalpies changes upon cycling using sample C30@PW; sample C42@PW shows the same tendency.

Table 1. Data for the thermal properties from DSC of the PCCs and PW.

Samples	Cycle times	*Melting process*				*Solidification process*			
		T_{mo} (°C)	T_{me} (°C)	T_{mp} (°C)	ΔH_m (J g^{-1})	T_{so} (°C)	T_{se} (°C)	T_{sp} (°C)	ΔH_s (J g^{-1})
PW	**5**	25.5	66.0	57.8	217.7	25.0	58.4	50.5	215.4
	100	25.5	66.0	57.8	217.7	25.0	58.4	50.5	215.3
C30@PW	**5**	27.4	76.0	62.0	182.8	21.5	57.8	45.2	179.6
	100	27.4	75.7	62.4	180.3	22.0	57.8	45.6	179.3
C42@PW	**5**	27.6	77.0	63.1	173.9	21.0	57.8	45.2	170.5
	100	27.6	76.1	63.1	173.7	21.0	58.0	45.7	169.4

T_{mo}, T_{me}, T_{mp}, ΔH_m are the onset point, end point, peak temperature and phase change enthalpy during the melting process, while T_{so}, T_{se}, T_{sp}, ΔH_s are the onset point, end point, peak temperature and phase change enthalpy during the solidification process, respectively.

3.5 Chemical stability test

The chemical stability of PW and PCCs were also confirmed by XRD and FT-IR analysis of the samples before and after cycling. Figure 9 shows the XRD patterns and FT/IR spectra of PW and the composite before/after cycling. The peaks for both XRD and FT-IR spectra are identical for all samples corresponding to the characteristic peaks of PW, illustrating the good chemical structure stability of paraffin upon repeated melting/solidification. It is noted that the peaks of carbon cloth are very weak since the carbon cloth are covered by PW in the composite. From the above results, the good chemical structure stability and good phase change stability of paraffin-based samples upon cycling can consolidate their usage for long-term TES through repeated thermal storage/release.

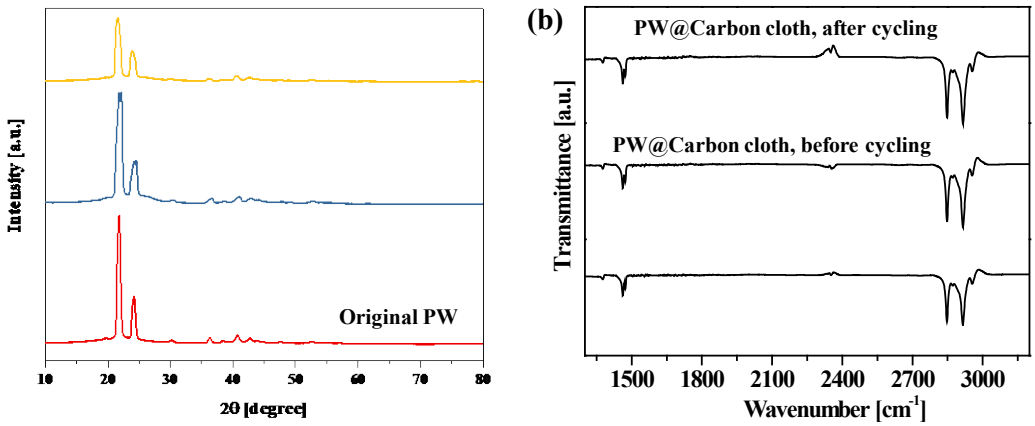

Figure 9. XRD patterns (a) and FT-IR spectra (b) of the PW and composite C42@PW before and after cycling test.

4. Conclusions

In summary, composite PCM using paraffin and textiled carbon supporting scaffold has been fabricated for thermal energy storage application. The highly thermal conductive and porous carbon scaffold with flexible shape was produced by the direct carbonization of cotton cloth. The porous supporting framework could help prevent paraffin from leakage by confining the liquid PCM within the hierarchical pore structure and enhance the heat transfer property by the 3D high thermally conductive network. The composite can present anisotropically improved thermal conductivity by aligning the carbon sheets in their main yarn direction. The thermal conductivity of the composite with a carbon weight ratio of 16.5wt% is increased to 0.99 W K^{-1} m^{-1} from the main yarn direction and 0.68 W K^{-1} m^{-1} from the through sheet direction, which are

greatly higher than the value of paraffin (0.25 W k^{-1} m^{-1}), and the composite also shows a high heat capacity of 170 J g^{-1}. The anisotropic thermal conductive property can reinforce the application of designing anisotropic heat transfer systems that could be needed, for example, in thermal dissipation of electronic devices. Combining the advantages, such as facile production of flexible and shapeable carbon supporting scaffold, high thermal storage capability, good shape-stability, high thermal conductivity and anisotropic thermal transfer property, the composite PCM can show advanced applications in solar thermal energy storage.

References:

[1] H. Nazir, M. Batool, F.J. Bolivar Osorio, M. Isaza-Ruiz, X. Xu, K. Vignarooban, P. Phelan, Inamuddin, A.M. Kannan, Recent developments in phase change materials for energy storage applications: A review, International Journal of Heat and Mass Transfer, 129 (2019) 491-523.
[2] G. Alva, L. Liu, X. Huang, G. Fang, Thermal energy storage materials and systems for solar energy applications, Renewable and Sustainable Energy Reviews, 68 (2017) 693-706.
[3] H. Chirino, B. Xu, X. Xu, P. Guo, Generalized diagrams of energy storage efficiency for latent heat thermal storage system in concentrated solar power plant, Applied Thermal Engineering, 129 (2018) 1595-1603.
[4] S. Kahwaji, M.B. Johnson, A.C. Kheirabadi, D. Groulx, M.A. White, Fatty acids and related phase change materials for reliable thermal energy storage at moderate temperatures, Solar Energy Materials and Solar Cells, 167 (2017) 109-120.
[5] X. Lu, C. Fang, X. Sheng, L. Zhang, J. Qu, One-step and solvent-free synthesis of polyethylene glycol-based polyurethane as solid-solid phase change materials for solar thermal energy storage, Industrial & Engineering Chemistry Research, (2019).
[6] J. Yang, L.-S. Tang, R.-Y. Bao, L. Bai, Z.-Y. Liu, W. Yang, B.-H. Xie, M.-B. Yang, Largely enhanced thermal conductivity of poly (ethylene glycol)/boron nitride composite phase change materials for solar-thermal-electric energy conversion and storage with very low content of graphene nanoplatelets, Chemical Engineering Journal, 315 (2017) 481-490.
[7] S. Shen, S. Tan, S. Wu, C. Guo, J. Liang, Q. Yang, G. Xu, J. Deng, The effects of modified carbon nanotubes on the thermal properties of erythritol as phase change materials, Energy Conversion and Management, 157 (2018) 41-48.
[8] L. Zhang, L. An, Y. Wang, A. Lee, Y. Schuman, A. Ural, A.S. Fleischer, G. Feng, Thermal enhancement and shape stabilization of a phase-change energy-storage material via copper nanowire aerogel, Chemical Engineering Journal, (2019).
[9] D. Zou, X. Ma, X. Liu, P. Zheng, Y. Hu, Thermal performance enhancement of composite phase change materials (PCM) using graphene and carbon nanotubes as additives for the potential application in lithium-ion power battery, International Journal of Heat and Mass Transfer, 120 (2018) 33-41.
[10] F. Wang, Z. Ling, X. Fang, Z. Zhang, Optimization on the photo-thermal conversion performance of graphite nanoplatelets decorated phase change material emulsions, Solar Energy Materials and Solar Cells, 186 (2018) 340-348.
[11] P. Lv, C. Liu, Z. Rao, Experiment study on the thermal properties of paraffin/kaolin thermal energy storage form-stable phase change materials, Applied Energy, 182 (2016) 475-487.
[12] Z. Rao, G. Zhang, T. Xu, K. Hong, Experimental study on a novel form-stable phase change materials based on diatomite for solar energy storage, Solar Energy Materials and Solar Cells, 182 (2018) 52-60.
[13] W. Lin, Q. Wang, X. Fang, X. Gao, Z. Zhang, Experimental and numerical investigation on the novel latent heat exchanger with paraffin/expanded graphite composite, Applied Thermal Engineering, 144 (2018) 836-844.
[14] A.B. Rezaie, M. Montazer, One-step fabrication of fatty acids/nano copper/polyester shape-stable composite phase change material for thermal energy management and storage, Applied Energy, 228

(2018) 1911-1920.
[15] Q. Zhang, J. Liu, Anisotropic thermal conductivity and photodriven phase change composite based on RT100 infiltrated carbon nanotube array, Solar Energy Materials and Solar Cells, 190 (2019) 1-5.
[16] J. Yang, L.-S. Tang, L. Bai, R.-Y. Bao, Z. Liu, B.-H. Xie, M.-B. Yang, W. Yang, Photodriven Shape-Stabilized Phase Change Materials with Optimized Thermal Conductivity by Tailoring the Microstructure of Hierarchically Ordered Hybrid Porous Scaffolds, ACS Sustainable Chemistry & Engineering, 6 (2018) 6761-6770.
[17] J. Yang, X. Li, S. Han, R. Yang, P. Min, Z.-Z. Yu, High-quality graphene aerogels for thermally conductive phase change composites with excellent shape stability, Journal of Materials Chemistry A, 6 (2018) 5880-5886.
[18] P. Zhang, Z.N. Meng, H. Zhu, Y.L. Wang, S.P. Peng, Melting heat transfer characteristics of a composite phase change material fabricated by paraffin and metal foam, Applied Energy, 185 (2017) 1971-1983.
[19] Y. Xia, W. Cui, H. Zhang, F. Xu, L. Sun, Y. Zou, H. Chu, E. Yan, Synthesis of three-dimensional graphene aerogel encapsulated n-octadecane for enhancing phase-change behavior and thermal conductivity, Journal of Materials Chemistry A, 5 (2017) 15191-15199.
[20] Y. Li, J. Li, W. Feng, X. Wang, H. Nian, Design and Preparation of the Phase Change Materials Paraffin/Porous Al2O3@Graphite Foams with Enhanced Heat Storage Capacity and Thermal Conductivity, ACS Sustainable Chemistry & Engineering, 5 (2017) 7594-7603.
[21] M.A. Palazzolo, M.-A. Dourges, A. Magueresse, P. Glouannec, L. Maheo, H. Deleuze, Preparation of Lignosulfonate-Based Carbon Foams by Pyrolysis and Their Use in the Microencapsulation of a Phase Change Material, ACS Sustainable Chemistry & Engineering, 6 (2018) 2453-2461.
[22] B. Wang, R. Karthikeyan, X.-Y. Lu, J. Xuan, M.K.H. Leung, Hollow Carbon Fibers Derived from Natural Cotton as Effective Sorbents for Oil Spill Cleanup, Industrial & Engineering Chemistry Research, 52 (2013) 18251-18261.
[23] H. Bi, Z. Yin, X. Cao, X. Xie, C. Tan, X. Huang, B. Chen, F. Chen, Q. Yang, X. Bu, X. Lu, L. Sun, H. Zhang, Carbon Fiber Aerogel Made from Raw Cotton: A Novel, Efficient and Recyclable Sorbent for Oils and Organic Solvents, Advanced Materials, 25 (2013) 5916-5921.
[24] C. Li, B. Xie, D. Chen, J. Chen, W. Li, Z. Chen, S.W. Gibb, Y. Long, Ultrathin graphite sheets stabilized stearic acid as a composite phase change material for thermal energy storage, Energy, 166 (2019) 246-255.